Syntheses, Structures, and Bonding of Boron Containing Niobium and Ruthenium Clusters Stabilized by Chalcogens

Subhash Bairagi, Debipada Chatterjee, Aishee De, Marie Cordier, Thierry Roisnel, Sundargopal Ghosh

Research Highlights

- Synthesis and structural characterization of boron containing niobium and ruthenium clusters stabilized by chalcogens.
- Theoretical investigations have been performed to understand the electronic structure and bonding scenario in these clusters.

Syntheses, Structures, and Bonding of Boron Containing Niobium and Ruthenium Clusters Stabilized by Chalcogens

Subhash Bairagi,[‡a] Debipada Chatterjee,[‡a] Aishee De,[a] Marie Cordier,[b] Thierry Roisnel,[b] and Sundargopal Ghosh*[a]

[a] *Department of Chemistry, Indian Institute of Technology Madras, Chennai 600 036, India*
Email : sghosh@iitm.ac.in

[b] *Univ Rennes, CNRS, Institut des Sciences Chimiques de Rennes, UMR 6226, F-35000 Rennes, France*

Keywords: boron, niobium, ruthenium, sulfur, selenium

ABSTRACT

In an effort to synthesize niobaheteroboranes and ruthenaheteroboranes, two different synthetic methods are developed. The reactions of [Cp*$NbCl_4$] (**1**) with chalcogenaborate ligands [$LiBH_2E_3$] (E = S, Se) were carried out under reflux conditions. The reaction with sulfur yielded a triniobium polysulfide cluster [$(Cp^*Nb)_3(\mu_3\text{-}S)_3\{B(OCH_3)\}(\mu\text{-}S)_3$] (**2**) in which a trithiaborate ligand $[S_3B(OCH_3)]^-$ is coordinated to Nb_3 framework in a cubane-type geometry. While the reaction with selenium generated a diniobium polyselenide cluster [$(Cp^*NbCl)_2(\mu\text{-}Se_2\text{-}\kappa^1Se{:}\kappa^2Se')_2(\mu\text{-}O)$] (**3**) in which two diselenide ligands $\{[Se_2]^{2-}\}$ are coordinated with both the metal centres in an unsymmetrical $\kappa^1{:}\kappa^2$ fashion. On the other hand, efforts were directed towards

expliciting the coordinative sulfur centres of a preformed *arachno*-ruthenaborane [(Cp*Ru)$_2$(B_3H_8)(CS_2H)] (*arachno*-**4)**, by carrying out the pyrolysis of *arachno*-**4** with excess [BH_3·THF]. The reaction led to the formation of sulfido stabilized *pileo* cluster *nido*-ruthenathiaborane [2,3-(Cp*Ru)$_2$(μ-H)(B_3H_6)S] (**5)**, *nido*-ruthenaborane [2,3-(Cp*Ru)$_2$(μ-H)(B_4H_5Me)] (**6)** and thiomethyl bridged *nido*-ruthenaborane [2,3-(Cp*Ru)$_2$(μ-SMe)(B_3H_6)] (**7)**. One of the key features of complex **5** is the presence of an unusual pentacoordinated sulfido ligand(μ_5-S). All the complexes have been characterized by multinuclear NMR, mass spectrometry and their structural architectures have been unambiguously established by single-crystal X-ray diffraction studies. In addition, theoretical investigations provided valuable insights into the electronic structures and bonding of these clusters.

1. Introduction

Boron is one of the most intriguing elements in the periodic table. Like its neighbour carbon, boron also exhibits the property of catenation.[1] Further, boron is electron deficient, favoring multicentre bonding, thereby building up interesting polyhedral clusters with various structural arrangements.[2,3] In parallel to polyhedral clusters, another class of transition metal boron complexes with single boron or low boron content is of current interest.[4] In the last sixty years, the chemistry of polyhedral boranes has been enriched by significant contributions from Hawthorne, Lipscomb, Muetterties, Boone and others.[1,5] On the other hand, the isolobal analogy has been extensively exploited in developing facile synthetic routes to generate heteroatom and metal fragment incorporated boron clusters.[2,6] Thereafter, the interest in metallaboranes and metallaheteroboranes has proliferated remarkably due to the utility of these clusters in numerous

applications ranging from polymer science, material chemistry, ceramics, and boron-neutron capture therapy.[7]

The chemistry of early and late metallaheteroborane complexes has received pragmatic consideration over the years, which predominantly deals with metallacarboranes. In this regard, Grimes and co-workers are the most prominent contributors in synthesizing and exploring the reactivities of a large number of metallacarboranes.[8] Apart from that, in the last few decades, clusters made of metal, boron, and chalcogens have emerged as a novel and diverse domain of organometallic chemistry. These compounds are collectively referred to as metallachalcogenaboranes and are useful due to their unique structures and bonding patterns.[9] Depending upon the nature of the metal centre, metallachalcogenaboranes may exist in a variety of structural frameworks, which include icosahedron, decaborane analogue, fused polyhedral, open cage triple-decker, cubane with a missing vertex, homocubane, bishomocubane, trishomocubane, tetrahomocubane, etc.[9-13] Moreover, there exists a clear correlation between the geometries of these clusters and their electron counts.[14,15] For example, when one or more vertices of metallaborane or borane clusters get replaced by the corresponding number of chalcogen atoms, we obtain isoelectronic and isostructural chalcogenated analogues of the parent clusters. Additionally, a number of hypoelectronic metallachalcogenaboranes have also been encountered.[9]

In the last two decades, our group has been a prolific contributor in synthesizing metallachalcogenaboranes containing group 5-9 metal fragments.[9,10b,d,11-13] In this regard, two synthetic approaches to generate such clusters are mainly employed. The first one involves the treatment of chalcogen, diaryl dichalcogenide, or carbon disulfide with an in-situ generated intermediate from the fast metathesis of [Cp*MCl_x] (M = transition metal) precursor with

[$LiBH_4$·THF].[16] The alternative approach involves the reaction of the metal precursor with chalcogenaborate ligands formed *in situ* from the treatment of [$LiBH_4$·THF] with chalcogen ([$LiBH_2E_3$]), dichalcogenide ([$LiBH_3EPh$]) (E = S, Se, Te) and CS_2.[12a,13,17] These synthetic approaches have enabled us to isolate complexes in which small borane fragments are stabilized in the coordination sphere of bimetallic or trimetallic frameworks. Recently, we have synthesized and structurally characterized the first ever classical diborane(5) fragment in the coordination sphere of a binuclear tantalum template.[18] Further, we have reported that the room temperature and thermolytic reactions of [$LiBH_2E_3$] with [Cp*MCl_4] (M = Nb, Ta) yield trimetallic polychalcogenide clusters that generally feature a homocubane or cubane type geometry with one missing vertex.[12a,19] On the other hand, the treatment of chalcogenaborate ligands with ruthenium precursors such as [Cp*$RuCl_2$]$_2$ or [(*p*-cy)$RuCl_2$]$_2$ affords bimetallic polychalcogenide homocubane type clusters.[13] Inspired by these results, we have attempted to synthesize metallachalcogenaboranes by altering these previous reaction methodologies. Herein, we report the reflux reaction of chalcogenaborate ligands with [Cp*$NbCl_4$] which results in a tri-niobium polysulfide cluster with a B-OCH_3 fragment and a di-niobium polyselenide cluster with an oxo bridge. On the other hand, in our pursuit of novel ruthenathiaboranes we carried out the thermolysis of reported *arachno*-[(Cp*Ru)$_2$(B_3H_8)(CS_2H)] with [BH_3·THF], which generated three diruthenium clusters.

2. Results and discussion

Reactivity of [Cp*$NbCl_4$] (1) with [$LiBH_2E_3$] (E = S or Se). In order to synthesize new niobaheteroboranes, a mixture of [Cp*$NbCl_4$] with four equivalents of [$LiBH_2E_3$], (E = S, Se) in toluene was refluxed for 24 hours (Scheme 1). The reaction with sulfur yielded orange solid **2** (17% yield) along with previously reported **II** and an inseparable mixture of **IV** and **V**.[19a,c] While

the reaction with selenium afforded yellow solid **3** (12% yield) along with previously reported clusters **I** and **III**.[19c] Subsequently, **2** and **3** were characterized by multinuclear spectroscopy, mass spectrometry, and single-crystal X-ray analyses.

(Scheme 1 near here)

Missing vertex cubane 2. Complex **2** was isolated as an orange solid in 17% yield. A singlet at 2.10 ppm was observed in the ^{1}H NMR spectrum of **2** indicating the presence of a single Cp* environment which was further supported by the ^{13}C NMR spectrum. Additionally, the ^{1}H NMR spectrum also showed a singlet at 3.25 ppm, while the ^{13}C NMR spectrum showed a peak at 59.8 ppm. Thus, the presence of a methoxy group was envisaged. On the other hand, a single peak was observed at 4.4 ppm in the ^{11}B NMR spectrum. Besides, the mass spectrum revealed a peak at m/z = 886.9039 corresponding to the molecular formula $C_{30}H_{45}Nb_3S_6B$. Although the NMR spectroscopy and mass spectrometry data gave some idea about the structure of **2**, they were not sufficient to propose the exact unambiguous structure. Therefore, single crystal X-ray diffraction analysis was carried out on a suitable crystal of **2**.

(Fig. 1 near here)

The solid state X-ray structure revealed **2** as a tri-niobium cluster with the molecular formula of $[(Cp^*Nb)_3(\mu_3\text{-}S)_3\{B(OCH_3)\}(\mu\text{-}S)_3]$ (Fig. 1). The tri-niobium core forms an equilateral triangle with nearly equal Nb-Nb bond lengths (3.1470(11) Å, 3.1470(11) Å, 3.151 Å) and equal Nb-Nb-Nb bond angles close to 60° (59.960°). The Nb-Nb bond distances in **2** are comparable to those in similar reported niobaheteroboranes.[19a,c,20a] Further, each of the three edges of the Nb_3 triangle is bridged by two monosulphide atoms. Out of the six monosulphide units, three units are further bridged by a $\{B(OCH_3)\}$ fragment. Thus, the Nb_3 framework is coordinated with a trithiaborate $[S_3B(OCH_3)]^-$ ligand. The B-S bond distances (1.934(15) Å, 1.955(9) Å, 1.955(9)

Å) are comparable to those in reported metallaheteroboranes featuring trithiaborate $\{S_3BR\}^-$.[12a,19b,c,20] On the other hand, the B-O bond distance of 1.414(14) Å is comparable to that in oxametallaboranes of group 5.[16b,21] It is to be noted that the source of the methoxy $\{OCH_3\}$ group may be attributed to the cleavage of tetrahydrofuran present in the reaction mixture.[16b,22] Additionally, we can view a three-fold axis of symmetry passing through the $\{B(OCH_3)\}$ fragment and the centre of the Nb_3-triangle. Therefore, **2** has a symmetric geometry that is in well-agreement with its spectroscopic data. The M-M bond distances and ^{11}B NMR signals in similar trimetallic clusters with a missing vertex homocubane and missing vertex cubane geometries have been enlisted in Table 1.

(Table 1 near here)

An interesting structural aspect of **2** is that it features a triangular trimetallic framework. Such metallic frameworks are stabilized due to σ, π, δ or φ bonding interactions between the metal atoms and have attracted immense interest lately due to their aromaticity and unique magnetic properties.[23] In this regard, Robinson's group have reported the first trigallane cluster which exhibits π aromaticity with 6 π electrons.[23a] Later Maestri and coworkers have synthesized a π aromatic tripalladium cluster with 2 π electrons while the groups of Sadighi, Freitag and Liddle have reported 2 electron σ aromatic trimetallic clusters.[23b-e] Furthermore, Dehnen's group has recently isolated a trigonal prismatic bismuth cluster which shows φ aromaticity.[23f] On the other hand, Harvey and coworkers, have isolated a trigadolinum cluster in which the σ bonding interaction among the 4f electrons of the three gadolinium centres gives rise to strong spin-spin coupling resulting in a high spin (S = 11) ground state.[23g] In the recent years, our group has isolated a series of tritantalum and triniobium clusters which are structurally analogous to **2** and in our recent report on triniobium clusters we have discovered through theoretical calculations

that these clusters also exhibit an aromatic ring current along the trimetallic framework.[12a,19] Thus, a study of the electronic structure and bonding scenario in **2** is of interest.

We carried out density functional theory (DFT) calculations at the b3lyp/def2-tzvp level of theory. The structural parameters of the optimized geometry of **2** were found to be in close agreement with those of the solid-state structure (Table S1). A molecular orbital (MO) analysis revealed that there is an extensive delocalization of the d orbitals of the three niobium centres in the HOMO, resulting in a strong bonding interaction along the tri-niobium framework (Fig. 2(a)). To investigate the presence of aromaticity along the trimetallic framework, we carried out NICS calculations.[24] The negative values of absolute isotropic magnetic shielding at the centroid of the Nb_3 ring [NICS(0)] and at 1 Å away from the centre on either sides [NICS(1) and NICS(-1)] were computed for **2**. All these values were numerically negative which suggest the presence of a diatropic ring current (Tables S4). Thus, aromaticity of the triniobium ring play a major role in the stabilization of **2**. Further, a natural bond orbital (NBO) analysis also supported the presence of strong Nb-Nb bonds with significant Wiberg Bond Indices (WBIs) (Table S1). On the other hand, HOMO-5 displayed the bonding scenario in the trithiaborate ligand (Fig. 2(b)). This was further illustrated in the Laplacian plot of electron density along the S2′-B1-S3 plane, which showed bond critical points (BCP) and bond paths connecting the two sulfur atoms with boron (Fig. 2(c)). Furthermore, NBO analysis also depicted the bonding of Nb1′ with S4 atom (Fig. 2(d)). Besides, natural charge analysis revealed that the boron and sulfur atoms possess positive charges and act as donors of electron density, while the three niobium centres act as acceptors and bear negative formal charges (Table S3).

(Fig. 2 near here)

Bimetallic polyselenide 3. Complex **3** was isolated as a yellow solid in 12% yield.The ^{1}H NMR spectrum of **3** showed a singlet at 2.09 ppm, suggesting the presence of a single Cp* environment which was further confirmed by the ^{13}C NMR spectrum. Further, no resonance was observed in the ^{11}B NMR. On the other hand, the mass spectrum revealed a peak at *m*/*z* = 918.6976. The spectroscopic data was insufficient to conclude the unequivocal structure, therefore, single crystal X-ray analysis was carried out on suitable crystals of **3**. Interestingly, the X-ray structure revealed **3** to be a bimetallic polyselenide cluster with molecular formula of $[(Cp^*NbCl)_2(\mu\text{-}Se_2\text{-}\kappa^1Se{:}\kappa^2Se')_2(\mu\text{-}O)]$ (Fig. 3). The two Cp*Nb centres are stabilized by two bridging diselenide $\{[Se_2]^{2-}\}$ units and a μ-oxo bridge. Additionally, as shown in Fig. 2, a two-fold axis of symmetry passes through the midpoint of the Nb-Nb bond and the μ-oxo atom. Therefore, **3** has a symmetric structure which is consistent with the spectroscopic data.

(Fig. 3 near here)

The Nb-Nb bond distance of 3.2039(15) Å in **3** is comparable with those in **2** and other reported niobaheteroboranes.[19a,c] In the two diselenide ligands, one selenium is coordinated with a single metal centre while the other one is bonded to both the metal centres. Thus, the diselenide ligand is coordinated to the bimetallic template in a μ-η^2: η^1 fashion. This type of diselenide linkage has been previously encountered in polyselenide clusters, such as $[Tl_4M_2Se_{11}]$ (M = Ta, Nb), $[(triphos)Rh(\mu\text{-}Se_2)_2Rh(triphos)]^{2+}$ and $[Mn_2(\mu\text{-}Se_2)_2(CO)_6]^{2-}$.[25] Moreover, the bond distances of Nb-Se (2.4876(10) Å, 2.7872(12) Å, 2.7460(11) Å) and Se-Se (2.3273(16) Å) in **3** are comparable with those in the reported polyselenide clusters.[25]

Polyselenide ligands are extremely versatile and can bind with the metal centres in various coordination modes depending upon electronic and steric factors.[26a] Due to this versatility, polyselenide ligands can form different kinds of compounds ranging from metal complexes,

clusters and also polymers. Although there are plenty of reports regarding synthesis of such compounds, their reaction chemistry has been relatively less explored. In this regard, Shieh and coworkers have reported the selective activation of O_2 and insertion of elemental selenium by a hexamanganese carbonyl selenide cluster $[Se_6Mn_6(CO)_{18}]^{4-}$.[26b] Further they have also reported the activation of C=O of acetone in a reaction of selenium-capped trichromium carbonyl cluster $[Se_2Cr_3(CO)_{10}]^{2-}$ with $Mn(CO)_5Br$ in acetone.[26c] Thus, the reaction chemistry of **3** is of interest but we were unable to explore that aspect due to its modest yield and air sensitivity.

Reactivity of *arachno*-4 with [BH_3·THF]. In an attempt to isolate metallachalcogenaboranes of late transition metal, we have explored the chemistry with various ruthenaboranes via a similar approach. Reaction of $[Cp^*RuCl_2]_2$ or $[(p\text{-cy})RuCl_2]_2$ with chalcogenaborate ligands $[LiBH_2E_3]$ (E = S or Se) in various reaction conditions led to the formation of known bimetallic polychalcogenide homocubane clusters along with a few air sensitive compounds which could not be isolated in their pure form.[13] Recently, we have synthesized an interesting bimetallic dithioformato ligand coordinated *arachno*-**4** from the reaction of *nido*-$[(Cp^*RuH)_2B_3H_7]$ with CS_2.[12b] In an objective to isolate metallachalcogenaboranes during the cluster expansion reaction, an elevated-temperature reaction of *arachno*-**4** with [BH_3·THF] was performed (Scheme 2). The reaction afforded yellow solid **5** (8% yield), yellow solid **6** (16% yield), and yellow solid **7** (14% yield). These complexes are characterized by spectroscopic and single-crystal X-ray analyses.

(Scheme 2 near here).

Ruthenathiaborane 5. Complex **5** was isolated as a yellow solid in 8% yield. The ^{1}H NMR spectrum of **5** shows a single intense signal at 1.83 ppm, indicating one type of Cp* ligand. ^{13}C NMR spectrum is also consistent with one type of Cp* ring. ^{11}B NMR spectrum shows peaks at 54.1 and -3.7 ppm which suggests the presence of two different types of boron environments.

Moreover, ^{1}H NMR spectrum displays peaks at -4.02, -13.39, and -15.68 ppm in the upfield region, indicating the presence of B-H-B, Ru-H-B, and Ru-H-Ru protons, respectively, in this molecule. The IR spectrum displays bands at 2467 cm^{-1} corresponding to the vibration of terminal B-H protons. The mass spectrum shows a molecular ion peak at m/z = 572.9718 corresponding to molecular formula $C_{20}H_{36}SB_2Ru_2K$. Further, to elucidate the structure of complex **5**, we have performed a single crystal X-ray analysis on a suitable crystal grown from the hexane solution at -5 °C.

(Fig. 4 near here)

The solid-state X-ray structure of **5**, shown in Fig. 4(a), evidently shows the core geometry as mono-capped *nido*-[2,3-$(Cp^*Ru)_2(\mu$-H)$(B_3H_6)S$]. The square pyramidal framework of **5** is similar to that observed for nido-$[(Cp^*RuH)_2B_3H_7]$, where the pyramidal BH vertex is replaced by a sulfur atom in **5**.[28] In addition, cluster **5** possesses an added BH fragment which caps the Ru_2S face. This is the first example of a capped ruthenathiaborane, where a sulfur atom is penta-coordinated in a *nido*-geometry. Some examples of penta-coordinated sulfido clusters **VI**-**X** are listed in Chart 1, where all the clusters are *closo,* unlike **5**.[29-31] The core geometry of **5** is similar to other mono-capped *nido* square-pyramidal clusters $[(Cp^*Ru)_2B_4H_7(\mu$-H)$]$[28], $[(Cp^*Ru)_3B_3H_7(\mu$-H)$]$[32] and other clusters[33] listed in Table 2. The Ru-Ru bond distance of 2.7738(10) Å in **5** is comparable to the Ru-Ru bond distance of 2.897(3) in $[(Cp^*Ru)_2(Me)(S_2B_2H_3)]$[34] and other clusters listed in Table 2. The Ru-S bond lengths (2.307 Å) are comparable to the Ru-$S_{sulfido}$ bond length in $[(Cp^*Ru)_2(Me)(S_2B_2H_3)]$ (2.333 Å) but slightly shorter than that of Ru-S bond in $[(Cp^*Ru)_2(\mu,\eta^1{:}\eta^1\text{-}S_2)(\mu\text{-}S_2BH\text{-}\kappa^1B{:}\kappa^2S{:}\kappa2S')]$ (2.450 Å).[34]

(Chart 1 near here)

The spectroscopic data nicely corroborate with the solid-state structure of **5**. For example, the $^{11}B\{^1H\}$ NMR chemical shifts of **5** for the capped boron atom appeared in the downfield region. The $^{11}B\{^1H\}$ resonances of **5** at 54.1 and -3.7 ppm are assigned to B1, and B2, B3, respectively. The *nido*-type structure was confirmed by the presence of bridging protons resonance upfield in ^1H NMR.

(Table 2 near here)

The MO analysis of **5** depicted that the HOMO is delocalized through Ru1, B1, and Ru2 centres along with the B2, S1, and B3 centres (Fig. 5(a)). The HOMO-10 of **5** disclosed the overlap of the d_z^2 orbital of the Ru1 atom with the *p* orbital of S1 and B1, indicating the bonding interaction between the Ru1, S1, and Ru2 centres and Ru1, B1, and Ru2 centres (Fig. 5(b)). The contour line diagram along B2-S1-B3 and S1-B1-Ru1 indicates the presence of strong B-S, Ru-S, and Ru-B bonds in the cluster framework (Fig. 5(d, e)). Further, Ru-H-B and B-H-B bonding interactions are sketched in HOMO-11 of **5** (Fig. 5(c)). The contour line diagram along Ru1-H4-Ru2 also confirmed the Ru-H-Ru interaction (Fig. 5(f)). Two distinct type of natural charges are observed on boron atoms *i.e.* 0.250 for B1, -0.421 and -0.369 for B2 and B3, respectively. On the other hand, a positive natural charge on sulfur atom (0.738) is observed by performing the NBO analysis of **5** (Table S3).

(Fig. 5 near here)

Note that the reaction described in Scheme 2 also yielded complex **6,** which is the analogue of $[(Cp^*Ru)_2B_4H_7(\mu\text{-}H)]$.[28] In addition, **6** is also analogous to **5** but has two electrons less compared to **5**. The molecular structure, relevant bond lengths, and bond angles of **6** are shown in Fig. 4(b), and other spectroscopic data of **6** is provided in the ESI.

Thiomethyl bridged ruthenaborane 7. Cluster **7** was isolated as a yellow solid in 14% yield.The ^{11}B NMR spectrum displays two peaks in 2:1 ratio at 19.8 and 62.3 ppm, i.e., the presence of a minimum of three boron in the cluster. Furthermore, ^{1}H NMR spectrum shows a single Cp* signal at 1.80 ppm suggesting presence of a single type of Cp* in the cluster which is additionally confirmed by ^{13}C NMR. The ^{1}H NMR spectrum also shows one type of B-H-B (-2.02 ppm) and one type of Ru-H-B (-13.41 ppm) protons in 1:2 ratio. The IR spectrum also shows peak at 2526 and 2431 cm^{-1}, indicating characteristics of B-H terminal stretches. The constitution of **7** was ascertained by the solid-state X-ray diffraction study.

The X-ray data shows **7** as a thiomethyl bridged half sandwich ruthenaborane [2,3-(Cp*Ru)$_2$(μ-SMe)(B$_3$H$_6$)] (Fig. 6). Complex **7** can be described as a nido-square pyramidal structure, isoelectronic and isostructural with nido-[2,3-(Cp*RuH)$_2$B$_3$H$_7$].[28] The compound was crystallized in the monoclinic space group P-1 and displayed a square pyramidal core. The structural features of **7** are comparable with *nido*-[2,3-(Cp*RuH)$_2$B$_3$H$_7$] and its derivatives.[28,35] Although the Ru-Ru and Ru-B bonds are comparable with *nido*-[2,3-(Cp*RuH)$_2$B$_3$H$_7$] but B-B bonds are significantly shorter than that observed in *nido*-[(Cp*RuH)$_2$B$_3$H$_7$]. Both the Ru-S bond distances are in the range of standard single bonds. Although a large number of sulfido/thiomethyl bridged bimetallic complexes are reported in the literature, most of them contain a disulfide linkage, as observed in [CpMoMn(CO)$_5$(μ-S$_2$)] and [{Mn(CO)$_3$}$_2$(μ-CO)(μ-S$_2$)] or two sulfido ligands as in the case of [Cp*M(PMe$_3$)(μ-S)$_2$M′(NO)Cp*] (M = Rh, Ir; M′ = Mo, W).[34,36-38] Except for a few examples, complexes with a single sulfido/thiomethyl bridged between two metal atoms are rare, in particular, when the metal centres are ruthenium.

(Fig. 6 near here)

The MO analysis shows that the HOMO-LUMO gap of **7** (3.40 eV) is higher as compared to that of **5**. The Ru-Ru bonding interaction is depicted in HOMO-3 of **7**, where the *d* orbitals of both the Ru centres are delocalized to form the Ru-Ru bond (Fig. 7(b)). This Ru-Ru bonding is also verified by WBI of 0.411. The HOMO is delocalized on Ru1-Ru2-B1 centres and B21-B22-B23 centres (Fig. 7(a)). In addition, NBO analysis shows the *3c-2e* B21-B22-B23 interaction and Ru2-B21 interactions (Fig. 7(d, e)). Moreover, HOMO-12 of **7** reveals the bonding interaction (*d-p*) of Ru1-S1 and Ru2-S1 bonds, which is also supported by the contour line diagram along the Ru2-S1-Ru1 plane (Fig. 7(c, f)).

(Fig. 7 near here)

Electron Counts and Structural Comparison. Electron count is an essential aspect of cluster chemistry since it can be used to understand the structural and electronic features of cluster compounds. In this regard, the electron counting rules developed by Wade and Mingos have been widely used for clusters containing transition metal and main group atoms.[14,15,27] Thus, using these rules as a basis, a discussion on the electron counts of clusters **2**, **3**, and **5-7** is of interest.

The geometry of **2** may also be described as a cubane with a missing vertex. According to Wade's rules, the stable electron count for an M_4E_4 type cubane is (15 × 4 + 5 × 4) = 80, in which there is no M-M or M-E bond present along the diagonals of the cube.[14,15] For the formation of one M-M bond, there is a loss of 2 electrons, while breaking one M-M bond causes a gain of 2 electrons.[15] In **2**, as one transition-metal vertex is missing and three M-M bonds are present, the total valence electron count for this molecule should be {80 – 18 × 1 - (2 × 3)} = 56. However, the actual electron count of **2** is {10 (NbCp*) × 3 + 4 (μ_3-S) × 3 + 2 (μ-S) × 3 + 2 {$B(OCH_3)$} × 1} = 50. Therefore, **2** is a hypo-electronic cluster. On the other hand, the structure

of **3** can be viewed as a fusion of two Nb_2Se_2 butterfly cores that are edge-fused through the Nb-Nb bond. Considering the Mingos Fusion formalism,[27] it should have [2 × {(14 × 2) + (4 × 2) + 6} – {(16 × 2) + 2}] = 50 cluster valence electrons. However, the actual electron count of **3** is [10 (NbCp*) × 2 + 6 (Se) × 4 + 1 (Cl) × 2 + 2 (μ-O) × 1] = 48. Therefore, **3** is also a hypo-electronic cluster.

The cluster core of both **5** and **6** is a mono-capped square pyramid having two transition metals and three main group elements analogous to $[(Cp^*Ru)_2B_4H_7(\mu\text{-}H)]$. Thus, in consistency with Williams-Wade's rules, they are expected to possess 44 valence electrons.[14] Although, **6** is exactly electronically saturated with 44 electrons, contrastingly the total number of valence electrons available in **5** is 46 [13 (Cp*Ru) × 2 + 4 (BH) × 2 + 1 (μ-H) ×4 + 6 (S) + 2 (*capped*-BH)]. This is because the replacement of the apical BH fragment in cluster $[(Cp^*Ru)_2B_4H_7(\mu\text{-}H)]$ by a S-atom as a vertex increases the total CVE count by two electrons in cluster **5**, where a lone pair of two electrons on sulfur atom may not be participating in cluster bonding. Therefore, cluster **5** is a hyperelectronic cluster unlike **6** and the other clusters listed in Table 2 all of which possess 44 valence electrons.

The core structure of **7** is that of a square pyramid. Unlike **5** and **6**, the structure of 7 does not have any extra capping instead of which there is a thiomethyl bridge. However, having a square pyramidal core with two transition metals and three main group elements, **7** is also expected to possess 44 valence electrons. The total number of valence electrons available in **7** are indeed 44 [13 (Cp*Ru) × 2 + 4 (BH) × 3 + 1 (μ-H) ×3 + 3 (μ-SMe)]. Thus **7** is exactly electronically saturated. Moreover, it is interesting to note here that the niobium clusters **2** and **3** are hypoelectronic while the ruthenium clusters **6** and **7** are obedient to the electron counting rules and cluster **5** is hyperelectronic.

UV-visible studies. The absorption patterns of these colored complexes **4**-**7** became of interest due to the presence of metals and heteroatoms. The UV-vis absorption spectra of all the complexes were measured in the range of 280-800 nm in CH_2Cl_2 solution at 298 K. All of them display the most intense peaks at higher energy regions 260-300 nm due to the π−π* transition of Cp* ligands which are characteristic for most of the Cp* based metal complexes.[39] The absorptions with λ>300 nm exhibit mainly one or two absorption bands, shown in Fig. 8. These comparatively low energy bands, around 342-422 nm, have been assigned to the charge transfer bands. To understand the transition involved in these molecular transitions, we have performed the TD-DFT calculations and computed absorption spectra matched well with the experimental data (Tables S5-S7, Fig. S27-S29). Complex **4** shows three absorption bands at 354, 444, and 548 nm. Due to the formation of complex **5** from complex **4**, the high wavelength region band at 548 nm vanishes, whereas blue shift is observed in case of the other two bands, which appear at 342 and 422 nm in complex **5**. Complexes **6** and **7** show only a broad band at 358 and 380 nm, respectively. These absorption bands in **5**-**7** can be assigned as metal-to-ligand charge-transfer (MLCT) transitions.

(Fig. 8 near here)

3. Conclusion

In summary, we have synthesized and structurally characterized a triniobium cluster comprising a trithiaborate ligand and a diniobium polyselenide cluster containing two uniquely coordinated diselenide ligands. DFT calculations illustrated the presence of an extensive delocalization of the *d*-orbitals of the three niobium centres producing a diatropic ring current along the tri-niobium

skeleton which stabilizes the molecule. In the latter context, we have discussed three bimetallic *nido*-clusters of ruthenium, one of which shows a unique penta-coordinated binding mode of sulfido ligand. Electron counting rules suggested that both the niobium clusters are hypoelectronic while out of the three ruthenium clusters, two are electronically saturated and one is hyperelectronic. Current efforts are being directed towards synthesizing novel early and late transition metallaheteroboranes by tuning the metal precursors or chalcogen containing borate ligands.

4. Experimental section

General procedures and instrumentation. All experimental manipulations were carried out under an inert atmosphere of argon using standard Schlenk line or glove box techniques. All the solvents were freshly distilled prior to use employing standard literature procedures. $[Cp^*NbCl_4]$[40], $Li[BH_2E_3]$[41] (E = S or Se), and $[(Cp^*Ru)_2(B_3H_8)(CS_2H)]$[12b] were synthesized according to the reported procedures. The commercially available reagents [$LiBH_4$·THF], sulfur powder, selenium powder and carbon disulfide were used as received from Sigma, Avra and Alfa Aesar. Thin layer chromatographic separation of the reaction mixtures was carried out making use of aluminum-supported silica gel TLC plates (Merck KGaA, Darmstadt, Germany) of 250 µm diameter. All the NMR spectra were recorded in a 500 MHz Bruker FT-NMR spectrometer (Bruker, Billerica, MA, USA) while the ESI mass spectra were recorded in a Bruker MicroTOF-II mass spectrometer (Bruker Daltonics, Bremen, Germany). A JASCO FT/IR-1400 spectrometer (JASCO, Easton, PA, USA)IR was used to record IR spectra. UV-vis spectra were recorded on a Thermo Scientific (Evolution 300) UV-vis spectrometer.

Synthesis of 2: In an oven-dried Schlenk tube, [Cp*$NbCl_4$] (**1**) (0.100 g, 0.27 mmol) was suspended in 15 mL of toluene. A THF solution of Li[BH_2S_3] (4 equivalents, 1.08 mmol) was prepared *in-situ* and transferred using a cannula into the Schlenk tube containing the toluene suspension of **1**. This reaction mixture was stirred and refluxed for 24 h after which the solvent was dried under reduced pressure. The resulting residue was then extracted in a (70:30 v/v) n-hexane/CH_2Cl_2 mixture and filtered through 3 cm celite layer. The volatiles were vacuum dried and the residue was subjected to thin layer chromatographic separation by eluting with a n-hexane/CH_2Cl_2 mixture (70:30 v/v) which yielded orange solid **2** (0.014 g, 17% yield) along with known orange solid **II** (0.010 g, 6% yield) and known yellow solid mixture of **IV** and **V** (0.019 g, 12% yield).

2: MS (ESI^+): *m/z* calculated for $C_{30}H_{45}Nb_3S_6B^+$ $[(M - OCH_3)]^+$: 886.9134, found: 886.9039; ^1H NMR [$CDCl_3$, 500 MHz, 22 ºC, ppm]: 2.10 (s, 45 H; 3×Cp*), 3.25 ppm (s, O-*Me*); $^{11}B\{^1H\}$ NMR [$CDCl_3$, 160 MHz, 22 °C, ppm]: 4.4 (br, 1B); $^{13}C\{^1H\}$ NMR [$CDCl_3$, 125 MHz, 22 ºC, ppm]: 13.2 ($C_5\mathit{Me}_5$), 59.8 (O-*Me*), 118.7 (C_5Me_5).

Synthesis of 3: In an oven-dried Schlenk tube, [Cp*$NbCl_4$] (**1**) (0.100 g, 0.27 mmol) was suspended in 15 mL of toluene. A THF solution of Li[BH_2Se_3] (4 equivalents, 1.08 mmol) was prepared *in-situ* and transferred using a cannula into the Schlenk tube containing the toluene suspension of **1**. This reaction mixture was stirred and refluxed for 24 h after which the solvent was dried under reduced pressure. The resulting residue was then extracted in a (70:30 v/v) n-hexane/CH_2Cl_2 mixture and filtered through 3 cm celite layer. The volatiles were vacuum dried and the residue was subjected to thin layer chromatographic separation by eluting with a n-hexane/CH_2Cl_2 mixture (70:30 v/v) which yielded yellow solid **3** (0.014 g, 12% yield) along with known brown solid **I** (0.012 g, 6% yield) and known green solid **III** (0.015 g, 7% yield).

3: MS (ESI^+): *m/z* calculated for $C_{21}H_{37}Cl_2Nb_2OSe_4N^+$ [(M + CH_3CN) + NH_4}]$^+$: 918.7081, found: 918.6976; ^1H NMR [$CDCl_3$, 500 MHz, 22 ºC, ppm]: 2.09 (s, 30 H; 2×Cp*), $^{13}C\{^1H\}$ NMR [$CDCl_3$, 125 MHz, 22 ºC, ppm]: 12.8 ($C_5\mathit{Me}_5$), 126.4 (C_5Me_5).

Synthesis of 5-7: In a oven-dried schlenk tube, *arachno*-**1** (0.100 g, 0.17 mmol) was taken in 15 ml of dry toluene and an excess amount of [BH_3.THF] (1.0 mL, 1.0 mmol) was added dropwise at ambient temperature. The reaction mixture was stirred under thermolysis condition for 24 hr at 80°C and colour changed from purple to dark brown. After that, the solution was evaporated under reduced pressure. Then extraction was done by n-hexane/dichloromethane (80:20 v/v) through 3 cm celite using a frit. After complete removal of the solvent, the residue was dried and subjected to thin layer chromatographic technique by using silica gel TLC plates for the separation of reaction mixture. Elution with a n-hexane/ CH_2Cl_2 (80:20 v/v) mixture yielded yellow solid **5** (0.007 g, 8%), yellow solid **6** (0.014 g, 16%), and yellow solid **7** (0.013 g, 14%).

5: MS (ESI^+) calcd. for $C_{20}H_{36}SB_2Ru_2K^+$ [(M - BH) + K]$^+$ *m/z* 572.0478, found 572.9718; ^1H NMR [$CDCl_3$, 500 MHz, 22 ºC, ppm]: 9.31 (br, 1H, B-H_t), 3.52 (br, 2H, B-H_t), 1.83 (s, 30H; 2×Cp*), -4.02 (br, 1H, B-*H*-B), -13.39 (br, 2H, M-*H*-B), -15.68 (br, 1H, M-*H*-M; $^{11}B\{^1H\}$ NMR [$CDCl_3$, 160 MHz, 22 °C, ppm]: -3.7 (br, 2B), 54.1 (br, 1B); $^{13}C\{^1H\}$ NMR [$CDCl_3$, 125 MHz, 22 ºC, ppm]: 11.5 (s, $C_5\mathit{Me}_5$), 95.2 (s, C_5Me_5); IR [CH_2Cl_2, $\bar{\upsilon}$, cm^{-1}]: 2467 (B-H_t); UV-Vis [CH_2Cl_2, λ, nm]: 342, 422.

6: MS (ESI^+) calcd. for $C_{21}H_{39}B_4Ru_2^+$ [M]$^+$ *m/z* 539.1632, found 539.1655; ^1H NMR [$CDCl_3$, 500 MHz, 22 ºC, ppm]: 10.07 (br, 1H, B-H_t), 5.26 (br, 2H, B-H_t), 1.78 (s, 15H; 1×Cp*),1.76 (s, 15H; 1×Cp*), 0.79 (s, 3H, B-*Me*),-2.40 (br, 1H, B-*H*-B), -12.31 (br, 2H, M-*H*-B), -15.48 (br, 1H, M-*H*-M; $^{11}B\{^1H\}$ NMR [$CDCl_3$, 160 MHz, 22 °C, ppm]: 21.5 (br, 2B), 34.8 (br, 1B), 122.9 (br,

1B); $^{13}C\{^{1}H\}$ NMR [$CDCl_3$, 125 MHz, 22 ºC, ppm]: 11.3, 11.5 (s, $C_5\mathit{Me}_5$), 92.4, 92.5 (s, C_5Me_5); IR [CH_2Cl_2, ῡ, cm^{-1}]: 2468, 2523 (B-H_t); UV-Vis [CH_2Cl_2, λ, nm]: 358.

7: MS (ESI^+) calcd. for $C_{21}H_{39}SB_3Ru_2^+$ $[M]^+$ *m/z* 559.1176, found 559.1159; ^{1}H NMR [$CDCl_3$, 500 MHz, 22 ºC, ppm]: 5.35 (br, 1H, B-H_t), 2.82 (br, 2H, B-H_t), 2.04 (s, 3H, S-*Me*), 1.80 (s, 30H; 2×Cp*), -2.02 (br, 1H, B-*H*-B), -13.41 (br, 2H, M-*H*-B); $^{11}B\{^{1}H\}$ NMR [$CDCl_3$, 160 MHz, 22 °C, ppm]: 19.8 (br, 2B), 62.3 (br, 1B); $^{13}C\{^{1}H\}$ NMR [$CDCl_3$, 125 MHz, 22 ºC, ppm]: 11.1 (s, $C_5\mathit{Me}_5$), 94.1 (s, C_5Me_5); IR [CH_2Cl_2, ῡ, cm^{-1}]: 2431, 2526 (B-H_t); UV-Vis [CH_2Cl_2, λ, nm]: 380.

Note that we were unable to come up with any reasonable reaction mechanism or pathway for the formation of the reported products. This is because the reactions in which the monoborane or modified borohydride reagents are employed typically proceed in an undefined and uncontrolled manner mostly involving fragmentation of starting materials and cluster growth/rearrangements. As a result, we often observe the formation of kinetically stable products followed by some thermodynamically stable ones. In addition, many unstable side products are also observed in such reactions. The reactions that have been reported here are also augmented by some unstable compounds which were very difficult to isolate due to their higher sensitivity and low yields.

Computational details: The molecules **2** and **4**-**7** were optimized in gaseous state using single crystal X-ray structure coordinates and solvent effects were ignored. The optimizations were carried out using the B3LYP[42] functional and the def2-TZVP[43] basis set, employing the *Gaussian 16 program*[44]. Frequency calculations were performed which confirmed all the optimized geometries as true minima. Nucleus Independent Chemical Shift (NICS)[24] indices were computed using gauge including atomic orbital (GIAO)[45] approach in Gaussian on the optimized structure at the same level of theory. The GIAO[45] approach was also used to compute

the NMR chemical shifts. Natural bond orbital (NBO) analysis was performed with the NBO partitioning scheme[46] and Wiberg bond indexes[47] were obtained from it. The electron density distribution function was analyzed by the QTAIM[48] method utilizing the *Multiwfn, V.3.6,* package[49]. All optimized structures and orbital graphics were visualized either using *GaussView*[50] or *Chemcraft*[51] software packages.

X-ray structure determination analysis details: Suitable X-ray quality crystals of **2**, **3**, **5**-**7** were grown by slow diffusion of a hexane-CH_2Cl_2 solution. A Bruker Kappa APEX-II CCD (**2**, **3** and **5**) or D8 VENTURE Bruker AXS (**6** and **7**) diffractometer bearing a graphite monochromated MoK_α (λ = 0.71073 Å) radiated at 296 K (**2** and **3**) or 150 K (**5**, **6** and **7**) was used to collect and integrate the crystal data of compounds **2**, **3** and **5**-**7**. Heavy atom methods were employed to solve the structures by making use of SHELXS-97 or SIR92, and structure refinement was achieved using SHELXL-2018/3.[52] Structures of the molecules were drawn with Olex2.[53] Crystallographic data have been deposited with the Cambridge Crystallographic Data Centre as supplementary publication nos. CCDC-2236345 (**2**), 2304050 (**3**), 2208846 (**5**), 2208847 (**6**) and 2208823 (**7**). These data can be obtained free of charge from the Cambridge Crystallographic Data Centre via www.ccdc.cam.ac.uk/data_request/cif.

(Table 3 near here)

ACKNOWLEDGMENT

We acknowledge the support of Exploratory Research funding, IIT Madras, Grant No. RF/2223/0528/CY/RFER/008224. S.B., D.C. and A.D. thank IIT Madras for fellowships. We express our gratitude to Dr. V. Ramkumar and Dr. B. Varghese for X-ray structure analyses and discussion. The computational facility of IIT Madras is gratefully acknowledged.

Author Contributions

[‡] These authors contributed equally.

Appendix A. Supplementary data

Supplementary data related to this article can be found at http://dx.doi.org

REFERENCES

[1] (a) W.N. Lipscomb, Boron Hydrides, Benjamin, New York, 1963; (b) E.L. Muetterties, Boron Hydride Chemistry, Academic Press, New York, 1975; (c) R. Borthakur, K. Saha, S. Kar, S. Ghosh, Coord. Chem. Rev. 399 (2019) 213021–213037.

[2] (a) T.P. Fehlner, J.-F. Halet, J.-Y. Saillard, Molecular Clusters, Cambridge University Press, Cambridge, A Bridge to Solid-State Chemistry, 2007; (b) A. De, Q. Zhang, B. Mondal, L.F. Cheung, S. Kar, K. Saha, L.S. Wang, S. Ghosh, Chem. Sci. 9 (2018) 1976–1981; (c) S. Kar, S. Ghosh, Borane Polyhedra beyond Icosahedron, in: D.M.P. Mingos (Ed.), Structure and Bonding, Springer, Berlin, Heidelberg, 2021; (d) S. Kar, A.N. Pradhan, S. Ghosh, Polyhedral Metallaboranes and Metallacarboranes, Comprehensive Organometallic Chemistry IV 9 (2022) 263–369 G. Parkin, K. Meyer, D. O'hare, Eds; (e) S. Ghosh, B.C. Noll, T.P. Fehlner, Dalton Trans. (2008) 371–378.

[3] (a) A. S Weller, d and f-Block Metallaboranes, Comprehensive Organometallic Chemistry III 3 (2006) 133–174 R. H. Crabtree, D. M. P. Mingos, Eds.; (b) D. Sharmila, B. Mondal, R. Ramalakshmi, S. Kundu, B. Varghese, S. Ghosh, Chem. Eur. J. 21 (2015) 5074–5083; (c) K. Yuvaraj, D.K. Roy, K. Geetharani, B. Mondal, V.P. Anju, P. Shankhari, V. Ramkumar, S. Ghosh, Organometallics 32 (2013) 2705–2712; (d) R.S. Anju, D.K. Roy, K.

Geetharani, B. Mondal, B. Varghese, S. Ghosh, Dalton Trans. 42 (2013) 12828–12831; (e) B. Mondal, R. Bag, S. Ghorai, K. Bakthavachalam, E.D. Jemmis, S. Ghosh, Angew. Chem. Int. Ed. 57 (2018) 8079–8083.

[4] (a) T.B. Marder, Z. Lin, Contemporary Metal Boron Chemistry I: Borylenes, Boryls, Borane σ-Complexes, and Borohydrides, in Structure and Bonding, Vol. 130; Springer: Berlin, 2008; (b) K. Saha, D.K. Roy, R.D. Dewhurst, S. Ghosh, H. Braunschweig Acc. Chem. Res. 54 (2021) 1260–1273; (c) D.K. Roy, B. Mondal, R.S. Anju, S. Ghosh, Chem. Eur. J. 21 (2015) 3640–3648; (d) R.S. Anju, D.K. Roy, K. Geetharani, B. Mondal, B. Varghese, S. Ghosh, Dalton Trans. 42 (2013) 12828–12831; (e) R.S. Anju, D.K. Roy, B. Mondal, K. Yuvaraj, C. Arivazhagan, K. Saha, B. Varghese, S. Ghosh, Angew. Chem. Int. Ed. 53 (2014) 2873–2877; (f) K. Saha, R. Ramalakshmi, S. Gomosta, K. Pathak, V. Dorcet, T. Roisnel, J.-F. Halet, S. Ghosh, Chem. Eur. J. 23 (2017) 9812–9820; (g) S.K. Bose, D.K. Roy, P. Shankhari, K. Yuvaraj, B. Mondal, A. Sikder, S. Ghosh, Chem. Eur. J. 19 (2013) 2337–2343.

[5] (a) W.N. Lipscomb, A.R. Pitochelli, M.F. Hawthorne, J. Am. Chem. Soc. 81 (1959) 5833–5834; b) J.L. Boone, J. Am. Chem. Soc. 86 (1964) 5036; (c) A.R. Pitochelli, M.F. Hawthorne, J. Am. Chem. Soc. 82 (1960) 3228–3229.

[6] (a) R. Hoffmann, Angew. Chem. Int. Ed. Engl. 21 (1982) 711–724; (b) M. Elian, M.L. Chen, D.M.P. Mingos, R. Hoffmann, Inorg. Chem. 15 (1976) 1148–1155.

[7] (a) A.K. Saxena, N.S. Hosmane, Chem. Rev. 93 (1993) 1081–1124; (b) R.N. Grimes, in: Comprehensive Organometallic Chemistry II, Elsevier, 1995, pp. 373–430; (c) C.E.

Housecroft, Adv. Organomet. Chem. 33 (1991) 1−50; (d) L.F. Tietze, U. Griesbach, U. Bothe, H. Nakamura, Y. Yamamoto, ChemBioChem 3 (2002) 219–225.

[8] (a) R.N. Grimes, Carboranes, 3rd ed., Elsevier, Oxford, UK, 2016; (b) I.B. Sivaev, Polyhedral Boranes and Carboranes, Comprehensive Organometallic Chemistry IV 9 (2022) 196–262 G. Parkin, K. Meyer, D. O'hare, Eds.

[9] K. Pathak, C. Nandi, S. Ghosh, Coord. Chem. Rev. 453 (2022) 214303.

[10] (a) F.F. di Biani, F. Laschi, P. Zanello, G. Ferguson, J. Trotter, G.M. O'Riordand, T.R. Spalding, J. Chem. Soc., Dalton Trans. (2001) 1520–1523; (b) C. Nandi, S. Kar, M. Zafar, K. Kar, T. Roisnel, V. Dorcet, S. Ghosh, Inorg. Chem. 59 (2020) 3537–3541; (c) M.J. Carr, M.G.S. Londesborough, A.R. Hamilton McLeod, J.D. Kennedy, Dalton Trans. (2006) 3624–3626; (d) C. Nandi, A. Roy, K. Kar, M. Cordier, S. Ghosh, Inorg. Chem. 61 (2022) 16750–16759.

[11] (a) A. Thakur, S. Sao, V. Ramkumar, S. Ghosh, Inorg. Chem. 51 (2012) 8322–8330; (b) K.K.V. Chakrahari, A. Thakur, B. Mondal, V. Ramkumar and S. Ghosh, Inorg. Chem. 52 (2013) 7923–7932.

[12] (a) S. Kar, K. Saha, S. Saha, B. Kirubakaran, V. Dorcet, S. Ghosh, Inorg. Chem. 57 (2018) 10896–10905; (b) R.S. Anju, K. Saha, B. Mondal, V. Dorcet, T. Roisnel, J.-F. Halet, S. Ghosh, Inorg. Chem. 53 (2014) 10527–10535; (c) S.K. Barik, C.E. Rao, K. Yuvaraj, R. Jagan, S. Kahlal, J.-F. Halet, S. Ghosh, Eur. J. Inorg. Chem. (2015) 5556–5562.

[13] (a) K. Saha, S. Gayen, U. Kaur, T. Roisnel, S. Ghosh, Dalton Trans. 50 (2021) 12990–13001; (b) U. Kaur, S. Jaiswal, S. Gayen, S. Ghosh, J. Organomet. Chem. 989 (2023) 122642.

[14] (a) K. Wade, Inorg. Nucl. Chem. Lett. 8 (1972) 559-562; (b) K. Wade, Adv. Inorg. Chem. Radiochem. 18 (1976) 1–66.

[15] (a) J.D. Kennedy, Prog. Inorg. Chem. 34 (1984) 211−434; (b) J.L. Stark, B. Harms, I.G. -Jimenez, K.H. Whitmire, R. Gautier, J.-F. Halet, J.-Y. Saillard, J. Am. Chem. Soc. 121 (1999) 4409–4418.

[16] (a) R.S. Dhayal, K.K.V. Chakrahari, B. Varghese, S.M. Mobin, S. Ghosh, Inorg. Chem. 49 (2010) 7741–7747; (b) D.K. Roy, S.K. Bose, K. Geetharani, K.K.V. Chakrahari, S.M. Mobin, S. Ghosh, Chem. Eur. J. 18 (2012) 9983–9991.

[17] (a) M.G. Chowdhury, S.K. Barik, K. Saha, K. Bakthavachalam, A. Banerjee, V. Ramkumar, S. Ghosh, Inorg. Chem. 57 (2018) 985–994; (b) S. Kar, S. Bairagi, K. Kar, T. Roisnel, V. Dorcet, S. Ghosh, Eur. J. Inorg. Chem. (2021) 4443–4451; (c) C. Nandi, K. Kar, S. Gayen, T. Roisnel, S. Ghosh, Inorg. Chem. 60 (2021) 12367–12376.

[18] K. Saha, S. Ghorai, S. Kar, S. Saha, R. Halder, B. Raghavendra, E. D. Jemmis, S. Ghosh, Angew. Chem. Int. Ed. 58 (2019) 17684–17689.

[19] (a) S. Kar, S. Bairagi, K. Saha, B. Raghavendra, S. Ghosh, Dalton Trans. 48 (2019) 4203–4210; (b) K. Saha, S. Kar, S. Ghosh, J. Indian Chem. Soc. 95 (2018) 729–742; c) S. Kar, D. Chatterjee, J. -F. Halet, S. Ghosh, Molecules 27 (2022) 7473–7485.

[20] (a) H. Brunner, G. Gehart, B. Nuber, J. Wachter, M.L. Ziegler, Angew. Chem. Int. Ed. 31 (1992) 1021–1023; (b) H. Kawaguchi, K. Tatsumi, Organometallics 16 (1997) 307–309.

[21] R. Prakash, A. De, B. Kirubakaran, S. Ghosh, Inorg. Chem. 57 (2018) 14748–14757.

[22] S. Pasynkiewicz, W. Buchowicz, A. Pietrzykowski, J. Organomet. Chem. 531 (1997) 121–124.

[23] (a) X.-W. Li, W.T. Pennington, G.H. Robinson, J. Am. Chem. Soc. 117 (1995) 7578–7579; (b) S. Blanchard, L. Fensterbank, G. Gontard, E. Lacote, G. Maestri, M. Malacria, Angew. Chem. Int. Ed. 53 (2014) 1987–1991; (c) T.J. Robilotto, J. Bacsa, T.G. Gray, J.P. Sadighi, Angew. Chem. Int. Ed. 51 (2012) 12077–12080; (d) K. Freitag, C. Gemel, P. Jerabek, I.M. Oppel, R.W. Seidel, G. Frenking, H. Banh, K. Dilchert, R.A. Fischer, Angew. Chem. Int. Ed. 54 (2015) 4370–4374; (e) J.T. Boronski, J.A. Seed, D. Hunger, A.W. Woodward, J. van Slageren, A.J. Wooles, L.S. Natrajan, N. Kaltsoyannis, S.T. Liddle, Nature 598 (2021) 72–75; (f) B. Peerless, A. Schmidt, Y.J. Franzke, S. Dehnen, Nat. Chem. 15 (2023) 347–356; (g) K. R. McClain, H. Kwon, K. Chakarawet, R. Nabi, J. G. C. Kragskow, N. F. Chilton, R. D. Britt, J. R. Long, B. G. Harvey, Journal of the American Chemical Society 145 (2023) 8996–9002.

[24] (a) Z. Chen, C.S. Wannere, C. Corminboeuf, R. Puchta, P.v.R. Schleyer, Chem. Rev. 105 (2005) 3842–3888; (b) C.A. Tsipis, Aromaticity/antiaromaticity in “bare” and “ligand-stabilized” rings of metal atoms, in: G. Parkin (Ed.) Metal-Metal Bonding, Structure and Bonding, Springer, Berlin, Heidelberg, 2010, Volume 136, pp. 217–274.

[25] (a) C.L. Teske, N. Lehnert, W. Bensch, Z. Anorg. Allg. Chem. 628 (2002) 2651–2655; (b) C.L. Teske, W. Bensch, Acta Cryst. E62 (2006) i26–i28, (c) C. Bianchini, D. Masi, C.

Mealli, A. Meli, M. Sabat, F. Vizza, Inorg. Chem. 27 (1988) 3716–3721, (d) S.C.O' Neal, W.T. Pennington, J.W. Kolis, Inorg. Chem. 29 (1990) 3134–3138.

[26] (a) M. G. Kanatzidis, S.-P. Huang, Coord. Chem. Rev. 130 (1994) 509–621, (b) M. Shieh, C.-H. Ho, W.-S. Sheu, H.-W. Chen, J. Am. Chem. Soc. 132 (2010) 4032–4033, (c) M. Shieh, C.-Y. Miu, Y.-Y. Chu, C.-N. Lin, Coord. Chem. Rev. 256 (2012) 637–694.

[27] D.M.P. Mingos, Acc. Chem. Res. 17 (1984) 311–319.

[28] X. Lei, M. Shang, T.P. Fehlner, J. Am. Chem. Soc. 121 (1999) 1275–1287.

[29] (a) R. Macías, M. Thornton-pett, J. Holub, T.R. Spalding, Y. Faridoon, B. Štíbr, J.D. Kennedy, J. Organomet. Chem. 693 (2008) 435–445; (b) S. Luaces, J. Bould, R. Macías, R. Sancho, P.G. Orduña, F.J. Lahoz, L.A. Oro, J. Organomet. Chem. 721-722 (2012) 23–30.

[30] (a) P. Kaur, M. Thornton-Pett, W. Clegg, J.D. Kennedy, Dalton Trans. (1996) 4155–4157; (b) M. Bown, X.L.R. Fontaine, N. Greenwood, J.D. Kennedy, Z. anorg. allg. Chem. 602 (1991) 17–29.

[31] K.K. Chakrahari, D. Sharmila, S.K. Barik, B. Mondal, B. Varghese, S. Ghosh, J. Organomet. Chem. 749 (2014) 188–196.

[32] X. Lei, M. Shang, T.P. Fehlner, Inorg. Chem. 37 (1998) 3900–3901.

[33] B. Joseph, S. Gomosta, S.K. Barik, S.K. Sinha, T. Roisnel, V. Dorcet, J.-F. Halet, S. Ghosh, J. Organomet. Chem. 865 (2018) 29–36.

[34] K. Saha, S. Kar, U. Kaur, T. Roisnel, S. Ghosh, Organometallics 39 (2020) 4362−4371.

[35] C.E. Rao, K. Yuvaraj, S. Ghosh, J. Organomet. Chem. 776 (2015) 123–128.

[36] (a) K. Hashizume, Y. Mizobe, M. Hidai, Organometallics 14 (1995) 5367–5376; (b) S. Dev, K. Imagawa, Y. Mizobe, G. Cheng, Y. Wakatsuki, H. Yamazaki, M. Hidai, Organometallics 8 (1989) 1232–1237.

[37] J. R. Lockemeyer, T.B. Rauchfuss, A.L. Rheingold, J. Am. Chem. Soc. 111 (1989) 5733–5738.

[38] (a). R.D. Adams, S. Miao, Organometallics 22 (2003) 2492–2497; (b) K. Arashiba, S. Matsukawa, S. Kuwata, T. Tanabe, M. Iwasaki, Y. Ishii, Organometallics 25 (2006) 560–562.

[39] P. Govindaswamy, Y.A. Mozharivskyj, M.R. Kollipara, Polyhedron 24 (2005) 1710–1716.

[40] T. Okamoto, H. Yasuda, A. Nakamura, Y. Kai, N. Kanehisa, N. Kasai, J. Am. Chem. Soc. 110 (1988) 5008–5017.

[41] (a) J.M. Lalancette, A. Frêche, R.Monteux, Can. J. Chem. 46 (1968) 2754–2757; (b) J.M. Lalancette, M. Arnac, Can. J. Chem. 47 (1969) 3695–3697.

[42] C. Lee, W. Yang, R.G. Parr, Phys. Rev. B: Condens. Matter Mater. Phys. 37 (1988) 785–789.

[43] (a) F. Weigend, R. Ahlrichs, Phys. Chem. Chem. Phys. 7 (2005) 3297–3305. (b) F. Weigend, Phys. Chem. Chem. Phys. 8 (2006) 1057–1065.

[44] M.J. Frisch, G.W. Trucks, H.B. Schlegel, G.E. Scuseria, M.A. Robb, J.R. Cheeseman, G. Scalmani, V. Barone, G.A. Petersson, H. Nakatsuji, X. Li, M. Caricato, A.V. Marenich, J. Bloino, B.G. Janesko, R. Gomperts, B. Mennucci, H.P. Hratchian, J.V. Ortiz, A.F. Izmaylov, J.L. Sonnenberg, D. Williams-Young, F. Ding, F. Lipparini, F. Egidi, J. Goings,

B. Peng, A Petrone, T. Henderson, D. Ranasinghe, V.G. Zakrzewski, J. Gao, N. Rega, G. Zheng, W. Liang, M. Hada, M. Ehara, K. Toyota, R. Fukuda, J. Hasegawa, M. Ishida, T. Nakajima, Y. Honda, O. Kitao, H. Nakai, T. Vreven, K. Throssell, J.A. Jr. Montgomery, J.E. Peralta, F. Ogliaro, M.J. Bearpark, J.J. Heyd, E.N. Brothers, K.N. Kudin, V.N. Staroverov, T.A. Keith, R. Kobayashi, J. Normand, K. Raghavachari, A.P. Rendell, J.C. Burant, S.S. Iyengar, J. Tomasi, M. Cossi, J.M. Millam, M. Klene, C. Adamo, R. Cammi, J.W. Ochterski, R.L. Martin, K. Morokuma, O. Farkas, J.B. Foresman, D.J. Fox, Gaussian, Inc., Wallingford CT, 2016.

[45] (a) F.J. London, J. Phys. Radium 8 (1937) 397–409; (b) R. Ditchfield, Mol. Phys. 27 (1974) 789–807; (c) K. Wolinski, J.F. Hinton; P. Pulay, J. Am. Chem. Soc. 112 (1990) 8251–8260.

[46] (a) A.E. Reed, L.A. Curtiss, F. Weinhold, Chem. Rev. 88 (1988) 899–926; (b) F. Weinhold, C.R. Landis, Valency and Bonding: A Natural Bond Orbital Donor-Acceptor Perspective, Cambridge University Press, Cambridge, UK, 2005; (c) R.B. King, Inorg. Chem. 38 (1999) 5151–5153; (d) R.B. King, Inorg. Chim. Acta 300 (2000) 537–544.

[47] K. Wiberg, Tetrahedron 24 (1968) 1083–1096.

[48] (a) R.F.W. Bader, Atoms in Molecules: a Quantum Theory; Oxford University Press: Oxford, U.K., 1990; (b) R.F.W. Bader, J. Phys. Chem. A. 102 (1998) 7314–7323; (c) R.F.W. Bader, Chem. Rev. 91 (1991) 893–928.

[49] T. Lu, F. Chen, J. Comput. Chem. 33 (2012) 580−592.

[50] GaussView, Version 3.09, II. R.T. Dennington Keith, J. Millam, K. Eppinnett, W.L. Hovell, R. Gilliland, Inc, Semichem, Shawnee Mission KS, 2003.

[51] G.A. Zhurko, http://www.chemcraftprog.com.

[52] (a) G.M. Sheldrick, Acta Cryst A 71 (2015) 3–8; (b) G.M. Sheldrick, SHELXS97 and SHELXL97. Program for Crystal Structure Solution and Refinement; University of Gottingen: Germany, 1997.

[53] O.V. Dolomanov, L.J. Bourhis, R.J. Gildea, J.A.K. Howard, H. Puschmann, J. Appl. Cryst. 42 (2009) 339–341.

Scheme 1. Syntheses of **2** and **3**. (μ-E in **2**, **I-III** have been omitted for clarity)

Scheme 2. Syntheses of metallaheteroborane complexes **5**-**7**.

Fig. 1. X-ray structure of **2**. Selected bond distances (Å) and bond angles (°). Nb1-Nb2 3.1470(11), Nb1'-Nb2 3.1470(11), Nb1-Nb1' 3.151, Nb1-S1 2.381(2), Nb1-S2 2.542(2), B1-S3 1.934(15), B1-O1 1.414(14), O1-C17 1.265(17); Nb1-Nb1'-Nb2 59.960, Nb1-S4-Nb1' 82.765, Nb1-S3-Nb1' 76.717, S2-B1-S3 102.4(5), S3-B1-O1 120.0(10), B1-O1-C17 113.636.

Fig. 2. (a) HOMO, (b) HOMO-5, (c) Contour line diagram of the Laplacian of the electron density of **2** along the S2′-B1-S3 plane. Dashed crimson lines indicate the negative values of $\nabla^2\rho(r)$, while dotted dark black lines indicate the positive values of $\nabla^2\rho(r)$. Bond paths are indicated by brown lines, while blue and orange dots indicate bond critical points (BCPs) and ring critical points (RCPs), respectively. (d) NBO showing bonding interaction between Nb1 and S4. Contour values for isosurface are ± 0.04 $(e/bohr^3)^{1/2}$.

Fig. 3. X-ray structure of **3**. Selected bond distances (Å) and bond angles (°). Nb1-Nb1' 3.2039(15), Nb1-O1 1.937(4), Nb1-Cl1 2.452(2), Nb1-Se1 2.4876(10), Nb1-Se2 2.787, Se1-Se2 2.3273(16); Nb1-O1-Nb1' 111.573, Nb1-Se2-Nb1' 70.763, Nb1-Se1-Se2 70.65(4), Nb1- Cl1'-Nb1' 109.595.

Fig. 4. X-ray structures of **5** (a) and **6** (b). Selected bond distances (Å) and bond angles (°). **5**: Ru1-Ru2 2.7738(10), Ru2-S1 2.313(12), Ru1-B1 2.06(3), B1-S1 1.79(2), B2-B3 1.765(19); Ru1-B1-Ru2 85.3(13), Ru1-S1-Ru2 74.4(4), Ru2-B2-B3 100.6(15), Ru1-Ru2-B2 75.348, B2-S1-B3 57.6(8). **6**: Ru1-Ru2 2.8629(11), Ru1-B1 2.054(10), Ru1-B2 2.220(10), Ru2-B4 2.251(9), B1-B2 1.721(13), B3-B4 1.831(12), B4-C22 1.597(13); Ru1-B1-Ru2 88.4(4), Ru1-B2-Ru2 80.1(3), Ru1-B3-B4 104.1(5), Ru1-Ru2-B4 76.603, B3-B2-B4 63.2(5).

Fig. 5. (a) HOMO, (b) HOMO-10 and (c) HOMO-11 of **3**. Contour values for isosurface are ±0.04 $(e/bohr^3)^{1/2}$. (d, e and f) Contour line diagram of the Laplacian of the electron density of **3** along the B2-S1-B3, S1-B1-Ru1, and Ru1-H61-Ru2 plane, respectively.

Fig. 6. X-ray structure of **7**. Selected bond distances (Å) and bond angles (°). Ru1-Ru2 2.8032(4), Ru2-B21 2.146(3), Ru1-B22 2.226(3), Ru1-S1 2.2950(7), B21-B22 1.745(4); Ru1-S1-Ru2 75.41(2), Ru1-B21-Ru2 81.58(10), Ru2-B23-B22 103.37(18), Ru1-Ru2-B23 76.15(9).

Fig. 7. (a) HOMO, (b) HOMO-3, (c) HOMO-12 of **7**. (d and e) NBOs showing B1-B2-B3 and Ru1-B1 interactions, respectively. Contour values for isosurface are ±0.04 $(e/bohr^3)^{1/2}$. (c) Contour line diagram of the Laplacian of the electron density of **7** along the Ru2–S1–Ru1 plane.

Fig. 8. Combined UV−vis spectra of **4**-**7** in CH_2Cl_2.

Chart 1. Examples of penta-coordinated sulfido clusters.

Table 1. M-M bond distances and ^{11}B NMR data of trimetallic polychalcogenide clusters with missing vertex homocubane or missing vertex cubane geometry.

Table 2. Comparison of structural parameters and ^{11}B NMR chemical shifts of **5** and **6** with other related compounds.[24,28,29]

Table 3. Crystallographic data of **2**, **3**, and **5**-**7**.

Scheme 1

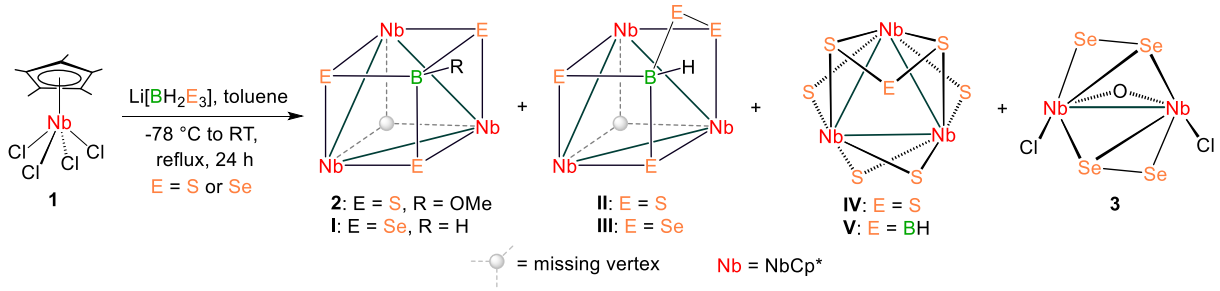

Scheme 2

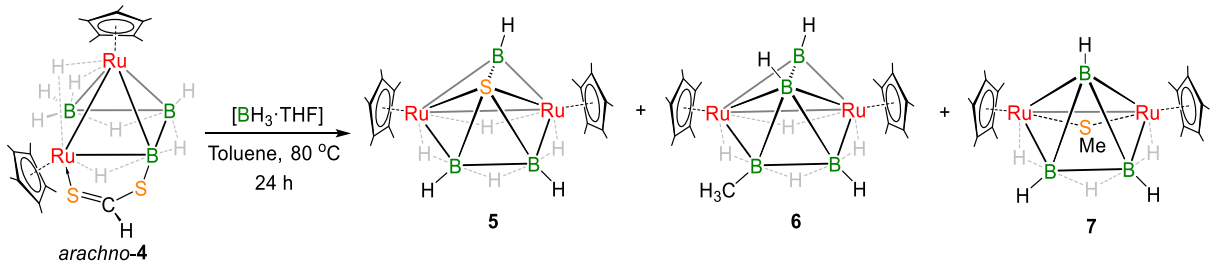

Fig. 1

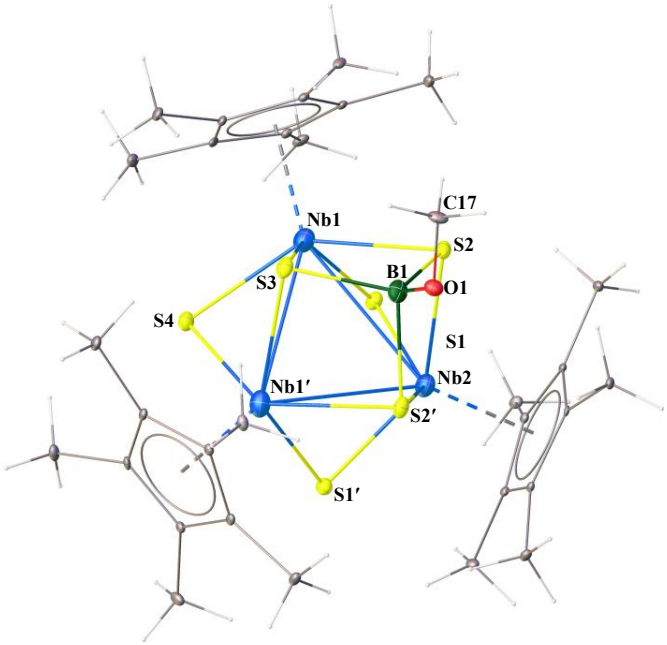

Fig. 2

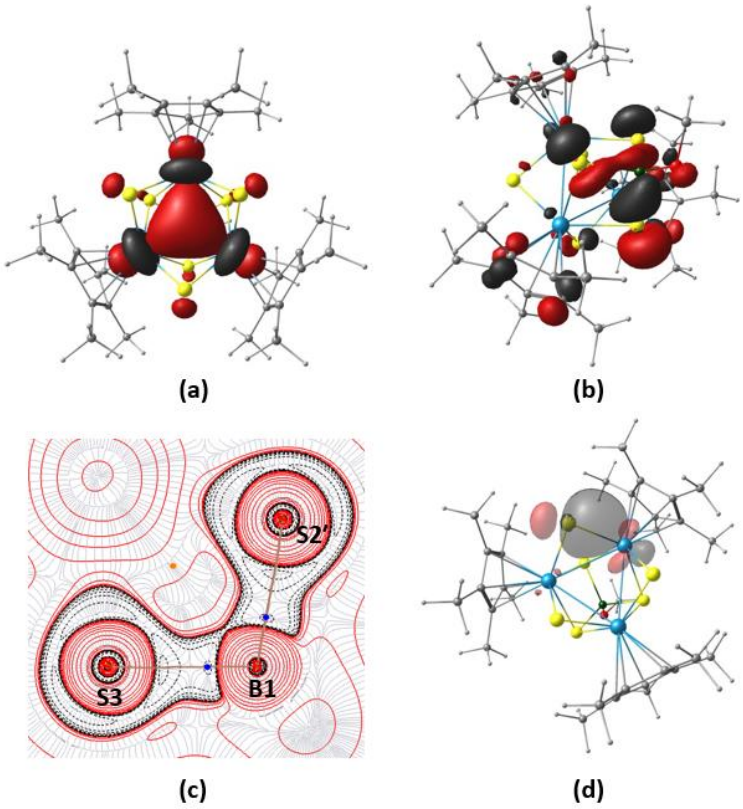

Fig. 3

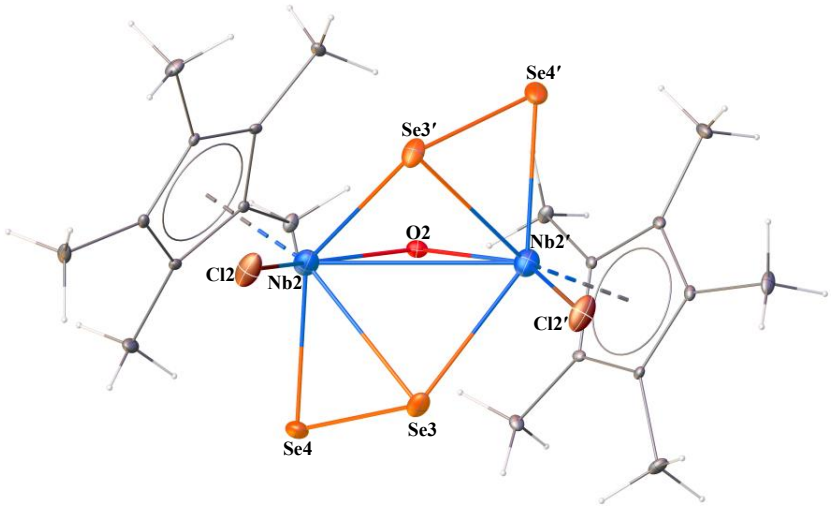

Fig. 4

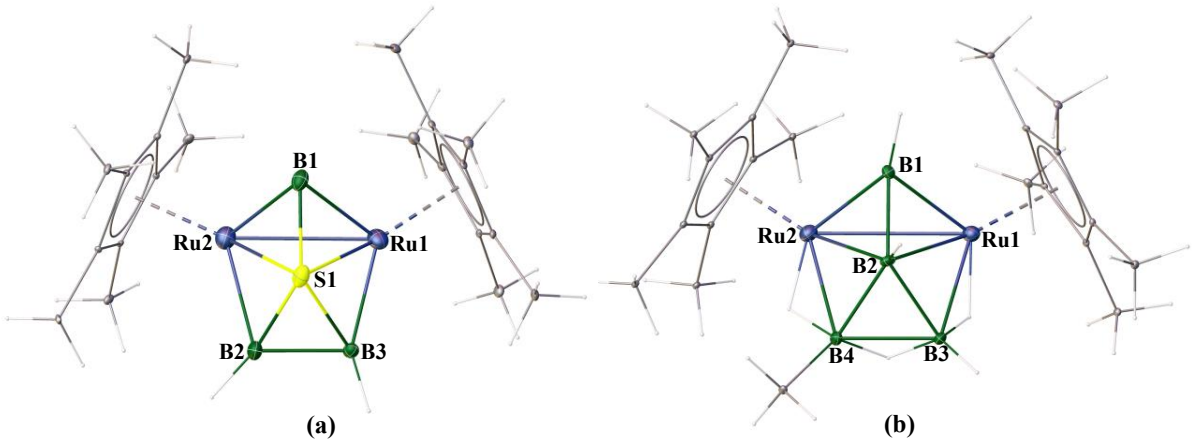

Fig. 5

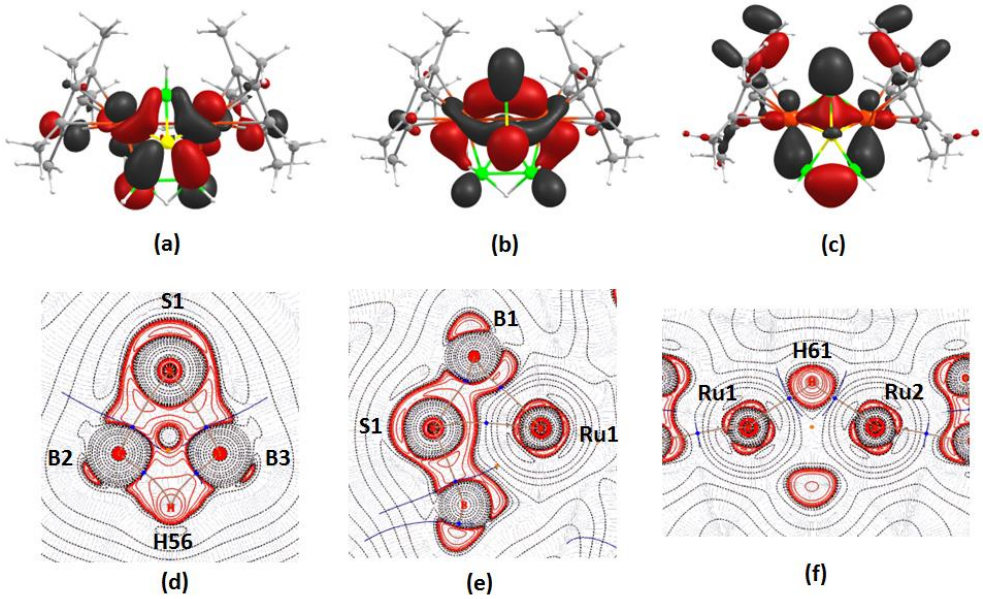

Fig. 6

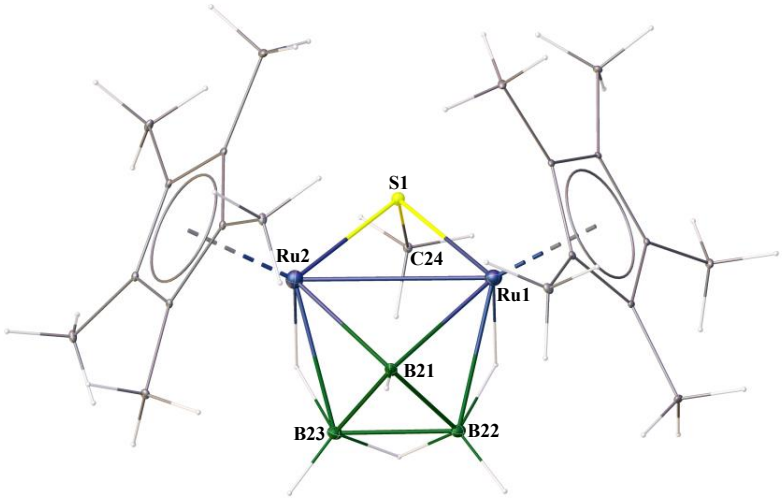

Fig. 7

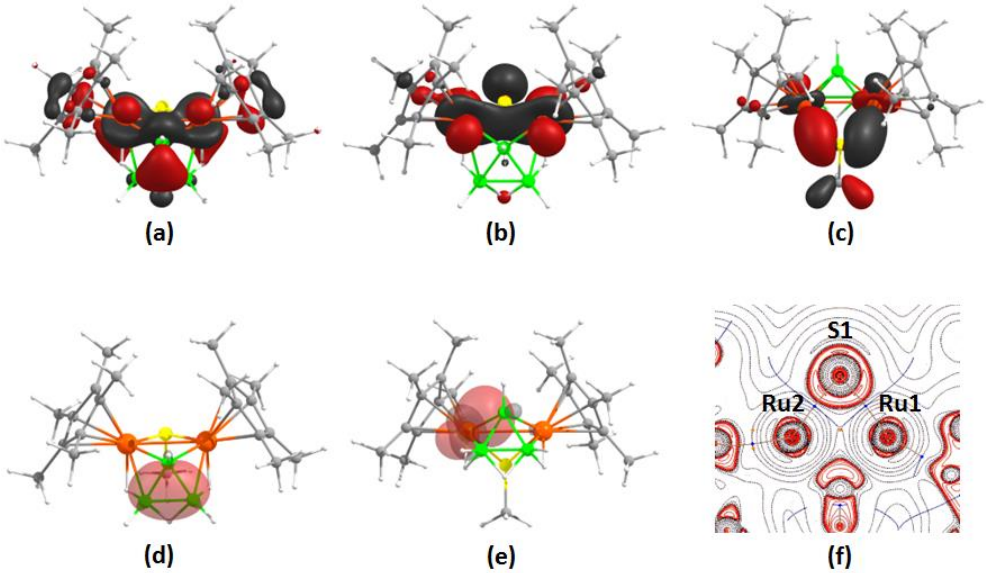

Fig. 8

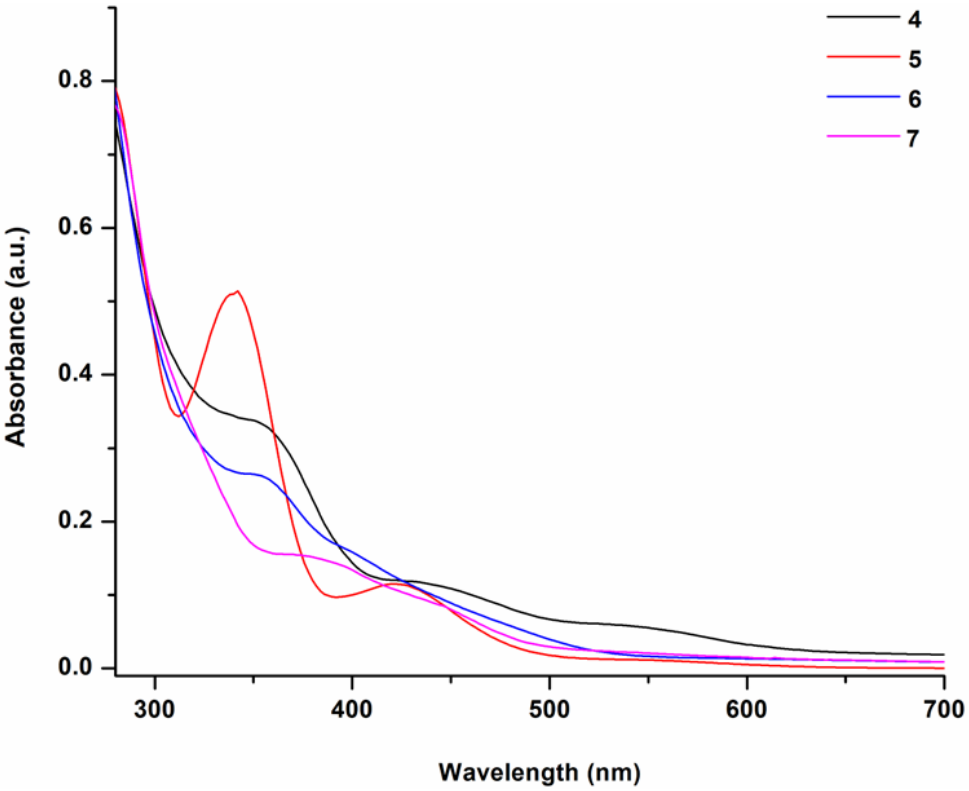

Chart 1

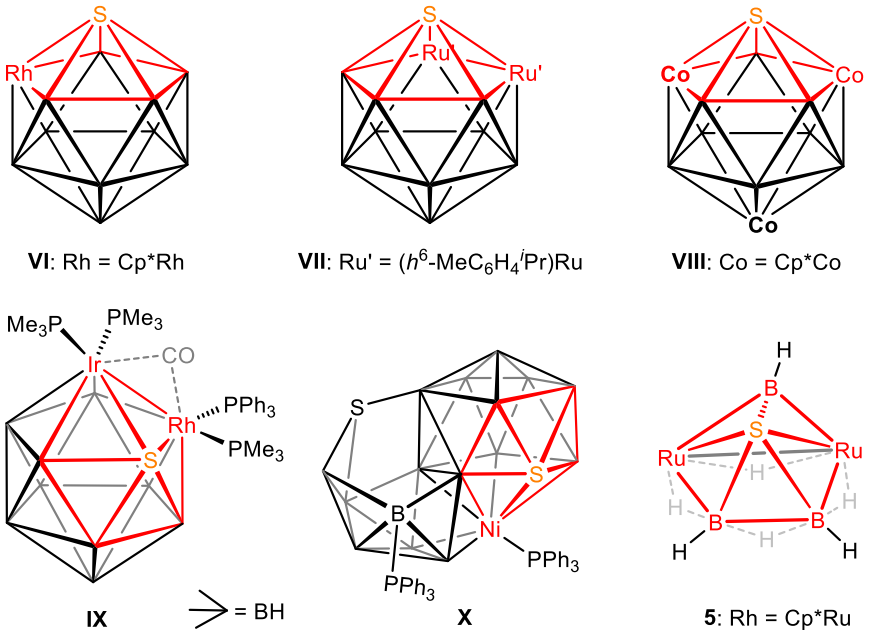

Table 1

Cluster	$d_{M\text{-}M}$ (Å)	^{11}B NMR	Cluster	$d_{M\text{-}M}$ (Å)	^{11}B NMR
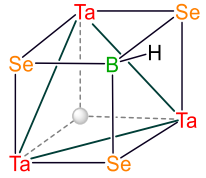	3.213(2) 3.2376(19) 3.213(2)	-11.2[12a]	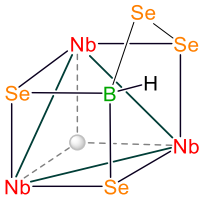	3.254(5) 3.307(4) 3.307(4)	-6.4[19c]
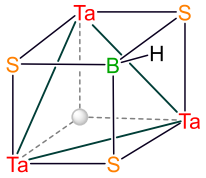	3.104(3) 3.095(3) 3.096(3)	-21.3[20b]	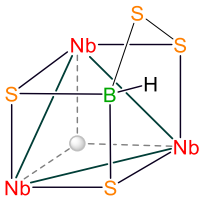	3.1750(9) 3.1750(9) 3.139(9)	-0.2[19a]
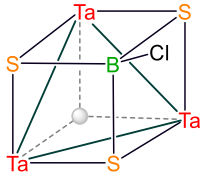	3.0953(4) 3.0967(4) 3.0910(4)	5.6[12a]	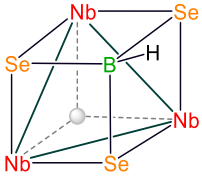	3.270(2) 3.271(2) 3.272(3)	-8.3[19c]
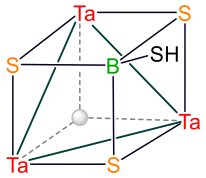	3.0974(6) 3.1153(6) 3.1054(7)	1.2[12a]	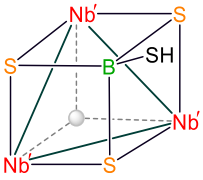	3.157(3) 3.157(3) 3.157(3)	1.9[20a]
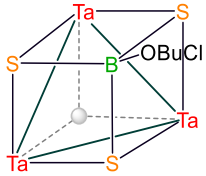	3.2291(18) 3.2368(18) 3.2402(5)	-5.5[19b]	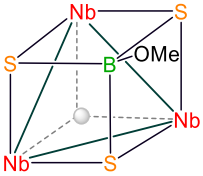	3.1470(11) 3.1470(11) 3.151	4.4[a]

Nb = Cp*Nb, Ta = Cp*Ta, Nb' = EtC_5Me_4Nb, [a]this work.

Table 2

Compound	$d_{M\text{-}M}$ [Å]	$d_{avg.B\text{-}B}$ [Å]	^{11}B NMR, [ppm]
$[(Cp^*Ru)_2B_4H_7(\mu\text{-}H)]$	2.855	1.720	-32.8, 21.3, 122.5
$[(Cp^*Ru)_2B_4H_7(Ph)]$	2.858	1.767	-31.6, 21.5, 33.8, 124.7
$[(Cp^*Ru)_2B_4H_7(Cl)]$	2.889	1.777	-10.8, 15.7, 128.8
$[(Cp^*Ru)_2B_4H_6(SPh)(Cl)]$	2.874	1.790	-7.9, 19.9, 23.0, 133.8
$[(Cp^*Ru)_3B_3H_7(\mu\text{-}H)]$	2.806	1.874	14.4, 128.3
$[(Cp^*Ru)_2B_3H_6S(\mu\text{-}H)]$, **5**	2.774	1.765	-3.7, 54.1
$[(Cp^*Ru)_2(B_4H_5Me)(\mu\text{-}H)]$, **6**	2.863	1.746	21.5, 34.8, 122.9

Table 3

	2	**3**	**5**	**6**	**7**
Empirical Formula	$C_{31}H_{48}BNb_3OS_6$ + CH_2Cl_2	$C_{20}H_{30}Cl_2Nb_2OSe_4$	$C_{20}H_{37}B_3Ru_2S$	$C_{21}H_{39}B_4Ru_2$	$C_{21}H_{39}B_3Ru_2S$
CCDC No.	2236345	2304050	2208846	2208847	2208823
Formula Weight	1003.52	859.00	544.12	536.90	558.15
Crystal System	monoclinic	monoclinic	monoclinic	triclinic	triclinic
Space Group	C2/m	C2	Cc	P-1	P-1
a(Å)	16.9576(15)	9.1572(3)	11.3251(10)	8.939(2)	8.4186(11)
b(Å)	14.1250(11)	14.5296(4)	13.9376(16)	9.401(2)	8.9416(12)
c(Å)	19.769(2)	20.5447(7)	15.4756(17)	16.171(4)	18.146(2)
α(Å)	90º	90º	90º	92.840(9)º	91.984(6)º
β(Å)	107.903(3)º	102.8727(14)º	103.189(4)º	104.628(9)º	97.826(6)º
γ(Å)	90º	90º	90º	113.290(9)º	117.594(5)º
V(Å^3)	4505.9(7)	2664.78(15)	2378.3(4)	1190.6(5)	1191.8(3)
Z	4	4	4	2	2
ρ_{calc} (g/cm^3)	1.479 g/cm^3	2.141	1.520	1.498	1.555
F(000)	2032.0	1640.0	1104.0	546.0	568.0
μ(mm^{-1})	1.170	6.535	1.360	1.272	1.359
2θ Range(°)	≤ 45.236	≤ 49.996	≤ 51.990º	≤ 55.282º	≤ 54.994º
no. of independent reflections	3137	4361	4439	5402	5424
no. of parameters	244	273	368	232	273
R_1	0.0486	0.0301	0.0487	0.0726	0.0268
wR_2	0.1084	0.0576	0.1216	0.2384	0.0638

Declaration of Interest Statement

The authors declare no competing financial interest.